Inorg. Chem. **2007**, *46*, 5979–5988

Evidence for Tetraphenylporphyrin Monoacids

Giovanna De Luca,[†] Andrea Romeo,[†] Luigi Monsù Scolaro,*[,†] Giampaolo Ricciardi,*[,‡] and Angela Rosa*[,‡]

Dipartimento di Chimica Inorganica, Chimica Analitica e Chimica Fisica, Università di Messina and C.I.R.C.M.S.B., Messina, Italy, and Dipartimento di Chimica, Università della Basilicata, Via N. Sauro 85, 85100 Potenza, Italy

Received February 21, 2007

Upon dilution from a concentrated solution in dichloromethane, the diacid form of tetraphenylporphyrin $\{H_4TPP(X)_2\}$ (X = Cl, PF_6 and tetrakis[3,5-bis(trifluoromethyl)phenyl]borate, TFPB) affords eventually the unprotonated free base species H_2TPP. At a difference of chloride, in the case of PF_6^- and $TFPB^-$ anions the conversion occurs with the intermediacy of a species, which has been assigned to a monoacid derivative on the basis of UV/vis absorption, fluorescence emission (static and dynamic), and resonance light scattering. Ground-state gas-phase geometries have been calculated both for the diacid $\{H_4TPP(PF_6)_2\}$ and monoacid $\{H_3TPP(PF_6)\}$ and $\{H_3TPP(Cl)\}$ species at the DFT/BP86 level of theory. TDDFT calculations using different functionals (BP86, SAOP, and B3LYP) have been exploited to provide electronic vertical excitation energies and oscillator strengths, yielding a remarkably good description of the optical spectra for these compounds and supporting the identification of the monoacid species. Gas-phase thermodynamic calculations on the chloride species provide an estimate of the Gibbs free energy changes associated with the two protonation steps, supporting the observed different behavior of this anion with respect to PF_6^- and $TFPB^-$.

Introduction

The acid−base behavior of porphyrins has been widely studied in the last 60 years largely because of the strong influence of the protonation state on their structural and photophysical properties.[1−4] This behavior depends, among other factors, on peripheral substitution, nature of the titrating acid or base, and dielectric constant of the solvent.[5−12] Generally, in the case of *meso*-aryl substituted porphyrins, the two protonation steps are almost indistinguishable, yielding the corresponding porphyrin dication (Scheme 1), while the monoprotonated species has not been usually detected.[2,5,7,13−15] To the best of our knowledge, only the monoacid derivative of a hydrocarbon-capped tetraphenylporphyrin has been reported and characterized in solution so far, taking advantage of a capping moiety on one face of the porphyrin plane.[16] In a few cases, the existence of these monoacid species was pointed out only by the lack of isosbestic points in UV/vis titrations or through kinetic

* To whom correspondence should be addressed. Phone: +39 090 676 5711 (L.M.S.), (+)39 0971 202238 (A.R. and G.R.). Fax: +39 090 393756 (L.M.S.), (+)39 0971 202223 (A.R. and G.R.). E-mail lmonsu@unime.it (L.M.S.), rg010sci@unibas.it (G.R.). Corresponding author address: Dipartimento di Chimica Inorganica, Chimica Analitica e Chimica Fisica, Università di Messina, Salita Sperone 31, 98166 Vill. S. Agata, Messina, Italy (L.M.S.), Dipartimento di Chimica, Università della Basilicata, Via N. Sauro 85, 85100 Potenza, Italy (A.R. and G.R.).

[†] Università di Messina and C.I.R.C.M.S.B.

[‡] Università della Basilicata.

(1) Aronoff, S.; Weast, C. A. *J. Org. Chem.* **1941**, *6*, 550−557.
(2) Stone, A.; Fleischer, E. B. *J. Am. Chem. Soc.* **1968**, *90*, 2735−2748.
(3) Gouterman, M. In *The Porphyrins*; Dolphin, D., Ed.; Academic Press: New York, 1978; Vol. 3, pp 1−165.
(4) Hambright, P. In *The Porphyrin Handbook*; Kadish, K. M., Smith, K. M., Guilard, R., Eds.; Academic Press: New York, 2000; Vol. 3, pp 129−210.
(5) Fleischer, E. B.; Webb, L. E. *J. Phys. Chem.* **1963**, *67*, 1131−1133.
(6) Meot-Ner, M.; Adler, A. D. *J. Am. Chem. Soc.* **1975**, *97*, 5107−5111.
(7) Karaman, R.; Bruice, T. C. *Inorg. Chem.* **1992**, *31*, 2455−2459.
(8) Rosa, A.; Ricciardi, G.; Baerends, E. J.; Romeo, A.; Scolaro, L. M. *J. Phys. Chem. A* **2003**, *107*, 11468−11482.
(9) De Luca, G.; Romeo, A.; Scolaro, L. M. *J. Phys. Chem. B* **2005**, *109*, 7149−7158.
(10) De Luca, G.; Romeo, A.; Scolaro, L. M. *J. Phys. Chem. B* **2006**, *110*, 7309−7315.
(11) De Luca, G.; Romeo, A.; Scolaro, L. M. *J. Phys. Chem. B* **2006**, *110*, 14135−14141.
(12) Garate-Morales, J. L.; Tham, F. S.; Reed, C. A. *Inorg. Chem.* **2007**, *46*, 1514−1516.
(13) Walter, R. I. *J. Am. Chem. Soc.* **1953**, *75*, 3860−3862.
(14) Hambright, P.; Fleischer, E. B. *Inorg. Chem.* **1970**, *9*, 1757−1761.
(15) Abraham, R. J.; Hawkes, G. E.; Smith, K. M. *Tetrahedron Lett.* **1974**, *15*, 71−74.
(16) Almarsson, O.; Blasko, A.; Bruice, T. C. *Tetrahedron* **1993**, *49*, 10239−10252.

10.1021/ic0703373 CCC: $37.00
Published on Web 06/23/2007

Scheme 1. Species Involved in the Acid−Base Equilibria of H_2TPP[a]

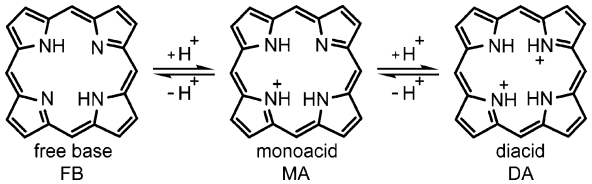

[a] Peripheral substituents and counteranions have been omitted for the sake of simplicity.

experiments.[17−27] Since the early days, the difficulty in observing these derivatives of *meso*-aryl substituted porphyrins has been ascribed to loss of symmetry which decreases resonance stabilization and to distortion of the porphyrin macrocycle, causing the monoprotonated species to exist over a very narrow pH range.[1,2,7,8,13−15,22−24,28−33] In particular, it has been suggested that the porphine core may suffer distortion as in diacids upon the first protonation. As a consequence of pyrrole tilting, the remaining nitrogen lone pair should be more accessible for the second proton attack.[2,23]

In the framework of our continuing interest in the protonation and aggregation behavior of porphyrins in organic solvents, we noticed that bulky and poorly coordinating anions show the ability to stabilize species with an intermediate state of protonation.[8−11] Here we report on the detection and spectroscopic characterization of the monoacid derivatives of tetraphenylporphyrin (H_2TPP) in dichloromethane solutions and on the dependence of their stability on the nature of the acid. Our experimental results are corroborated by density functional theory (DFT) and time-dependent DFT (TDDFT) calculations.

Experimental Section

Chemicals. Silver hexafluorophosphate and hydrochloric acid were purchased from Aldrich Chemical Co. and used as received. Sodium tetrakis[3,5-bis(trifluoromethyl)phenyl]borate and the corresponding acid (NaTFPB and HTFPB, respectively) were prepared according to a literature procedure.[34] Tetraphenylporphyrin (H_2-TPP) and its chloride salt $\{H_4TPP(Cl)_2\}$ were prepared and purified according to literature procedures,[8,35] while $\{H_4TPP(TFPB)_2\}$ was prepared by adding small amounts of HTFPB dichloromethane solutions to H_2TPP. $\{H_4TPP(PF_6)_2\}$ was prepared by adding stoichiometric amounts of $AgPF_6$ to a dichloromethane solution of $\{H_4TPP(Cl)_2\}$. The chloride anion was then removed as AgCl precipitate by filtration over cellulose powder. An analogous procedure was used to prepare $\{H_4TPP(TFPB)_2\}$, by adding NaTFPB to the $\{H_4TPP(Cl)_2\}$ solution and removing NaCl by filtration. The solvent was removed in vacuo. Spectrophotometric grade dichloromethane (Sigma) was distilled from BaO and eluted on activated alumina. Stock solutions of these species were prepared in freshly purified dichloromethane, stored in the dark, and used within a day of preparation. The range of concentration (10^{-3}−10^{-6} M) used in our experiments was determined spectrophotometrically using the molar extinction coefficient at the Soret maxima (H_2TPP: $4.78 \times 10^5\ M^{-1}\ cm^{-1}$, $\lambda = 419$ nm;[2] $\{H_4TPP(Cl)_2\}$: $4.31 \times 10^5\ M^{-1}\ cm^{-1}$, $\lambda = 445$ nm;[2] $\{H_4TPP(PF_6)_2\}$: $4.39 \times 10^5\ M^{-1}\ cm^{-1}$, $\lambda = 438$ nm, $\{H_4TPP(TFPB)_2\}$: $4.57 \times 10^5\ M^{-1}\ cm^{-1}$, $\lambda = 441$ nm).

Spectroscopic Methods. UV/vis absorption spectra were measured on a Hewlett-Packard Model HP 8453 diode array spectrophotometer, using cells of different path lengths (0.1−60 mm) depending on the concentration of the solutions. Fluorescence (emission and excitation) and resonance light scattering (RLS) spectra were recorded on a Jasco Model FP-750 spectrofluorimeter equipped with a Hamamatsu R928 photomultiplier (PMT). Both emission and excitation spectra have been normalized to 1. For RLS experiments a synchronous scan protocol with a right angle geometry was adopted.[36] 3D fluorescence experiments (see the Supporting Information) were carried out by means of the apposite Jasco software module, which perform an excitation of the sample at different wavelengths in a given range (excitation scan range), automatically recording the corresponding emission spectrum (in the emission scan range). The *data pitch* defines the scan resolution of emission and excitation ranges. For those emission spectra excited at wavelengths which fall into the emission scan range, *λ limiter* sets the minimum distance between the excitation wavelength and the starting wavelength of the emission scan range, to avoid the PMT to be saturated by reflections. Fluorescence lifetimes have been measured by a time-correlated-single-photon-counting (TCSPC) homemade apparatus with an experimental resolution of 50 ps.[37] Fluorescence and RLS spectra were not corrected for absorption of the samples, and a front-face geometry was adopted in the cases of the most concentrated solutions. Fluorescence emission was filtered with a high-pass filter (cutoff: 600 nm) to remove excitation overtones. A UV filter (Hoya glass type UV-34, cutoff: 340 nm) was used in all measurements in order to cut off the UV component of the instruments light sources, avoiding the formation of HCl by photodecomposition of dichloromethane.[38] The absorption spectra reported in Figures 1, 2a, 3a, and 4 have been normalized for the total porphyrin concentration and the optical

(17) Aronoff, S.; Calvin, M. *J. Org. Chem.* **1943**, *8*, 205−223.
(18) Aronoff, S. *J. Phys. Chem.* **1958**, *62*, 428−431.
(19) Pasternack, R. F.; Huber, P. R.; Boyd, P.; Engasser, G.; Francesconi, L.; Gibbs, E.; Fasella, P.; Cerio Venturo, G.; Hinds, L. D. *J. Am. Chem. Soc.* **1972**, *94*, 4511−4517.
(20) Baker, H.; Hambright, P.; Wagner, L. *J. Am. Chem. Soc.* **1973**, *95*, 5942−5946.
(21) Lavallee, D. K.; Gebala, A. E. *Inorg. Chem.* **1974**, *13*, 2004−2008.
(22) Hibbert, F.; Hunte, K. P. P. *J. Chem. Soc., Chem. Commun.* **1975**, 728−729.
(23) Pasternack, R. F.; Sutin, N.; Turner, D. H. *J. Am. Chem. Soc.* **1976**, *98*, 1908−1913.
(24) Hibbert, F.; Hunte, K. P. P. *J. Chem. Soc., Perkin Trans.* **1977**, *2*, 1624−1628.
(25) Jackson, A. H. In *The Porphyrins*; Dolphin, D., Ed.; Academic Press: New York, 1978; Vol. 1, pp 341−364.
(26) Barber, D. C.; Freitag-Beeston, R. A.; Whitten, D. G. *J. Phys. Chem.* **1991**, *95*, 4074−4086.
(27) Barber, D. C.; Woodhouse, T. E.; Whitten, D. G. *J. Phys. Chem.* **1992**, *96*, 5106−5114.
(28) Navaza, A.; de Rango, C.; Charpin, P. *Acta Crystallogr. Sect. C: Cryst. Struct. Commun.* **1983**, *39*, 1625−1628.
(29) Sutter, T. P. G.; Hambright, P. *Inorg. Chem.* **1992**, *31*, 5089−5093.
(30) Senge, M. O.; Forsyth, T. P.; Nguyen, L. T.; Smith, K. M. *Angew. Chem., Int. Ed.* **1995**, *33*, 2485−2487.
(31) Barkigia, K. M.; Fajer, J.; Berber, M. D.; Smith, K. M. *Acta Crystallogr. Sect. C: Cryst. Struct. Commun.* **1995**, *51*, 511−515.
(32) Cheng, B.; Munro, O. Q.; Marques, H. M.; Scheidt, W. R. *J. Am. Chem. Soc.* **1997**, *119*, 10732−10742.
(33) Yu, J.; Yu, B. S.; Cheong, K.; Choi, H.; Yu, S. C. *Bull. Korean Chem. Soc.* **1998**, *19*, 439−444.
(34) Brookhart, M.; Grant, B.; Volpe, A. F. J. *Organometallics* **1992**, *11*, 3920−3922.
(35) Adler, A. D.; Longo, F. R.; Finarelli, J. D.; Goldmacher, J.; Assour, J.; Korsakoff, L. *J. Org. Chem.* **1967**, *32*, 476.
(36) Pasternack, R. F.; Collings, P. J. *Science* **1995**, *269*, 935−939.
(37) Castriciano, M. A.; Romeo, A.; Villari, V.; Angelini, N.; Micali, N.; Scolaro, L. M. *J. Phys. Chem. B* **2005**, *109*, 12086−12092.
(38) Scolaro, L. M.; Romeo, A.; Castriciano, M. A.; De Luca, G.; Patanè, S.; Micali, N. *J. Am. Chem. Soc.* **2003**, *125*, 2040−2041.

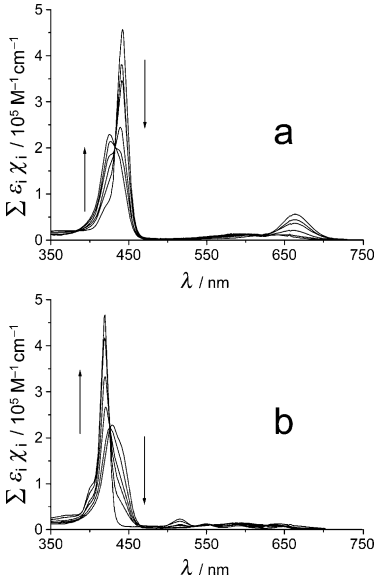

Figure 1. UV/vis spectral changes upon dilution of a dichloromethane solution of $\{H_4TPP(TFPB)_2\}$. Total H_2TPP concentration: (a) from 5.10×10^{-4} M to 2.66×10^{-5} M and (b) from 2.66×10^{-5} M to 2×10^{-7} M. Spectra have been normalized with respect to optical path length and total porphyrin concentration (see the Experimental Section).

path length of the cells. In the above-mentioned figures, the function plotted versus wavelength corresponds to the sum of the extinction coefficients of each porphyrin in a given protonation stage (ϵ_i) times the corresponding amount, as ratio to the total porphyrin concentration (χ_i). Deconvolution of UV/vis spectra has been performed by using PeakFit version 4.0 (SPSS Inc).

Computational Methods. The ground-state gas-phase geometries of $\{H_4TPP(PF_6)_2\}$, $\{H_3TPP(PF_6)\}$, $\{H_3TPP(Cl)\}$, and HCl were optimized at the DFT level using the BP86 functional.[39,40] H_2TPP and $\{H_4TPP(Cl)_2\}$ geometries optimized at the same level of theory were taken from ref 8. All optimized structures were verified to correspond to local minima by frequency analyses. Electronic vertical excitation energies and oscillator strengths were computed using TDDFT methods.[41−46] For the TDDFT calculations both pure (BP86 and the more elaborate, asymptotically correct, SAOP)[47,48] and hybrid (B3LYP)[49,50] functionals were examined. The BP86 and SAOP calculations were performed with the Amsterdam Density Functional (ADF) package[51,52] using the extensive TZ2P basis set, while TDDFT/B3LYP calculations were performed with Turbomole version 5.7.1[53] using the Karlsruhe split-valence basis set[54] augmented with polarization functions[55] (SVP).

Gas-phase thermodynamic calculations were performed with ADF using the BP86 optimized structures.

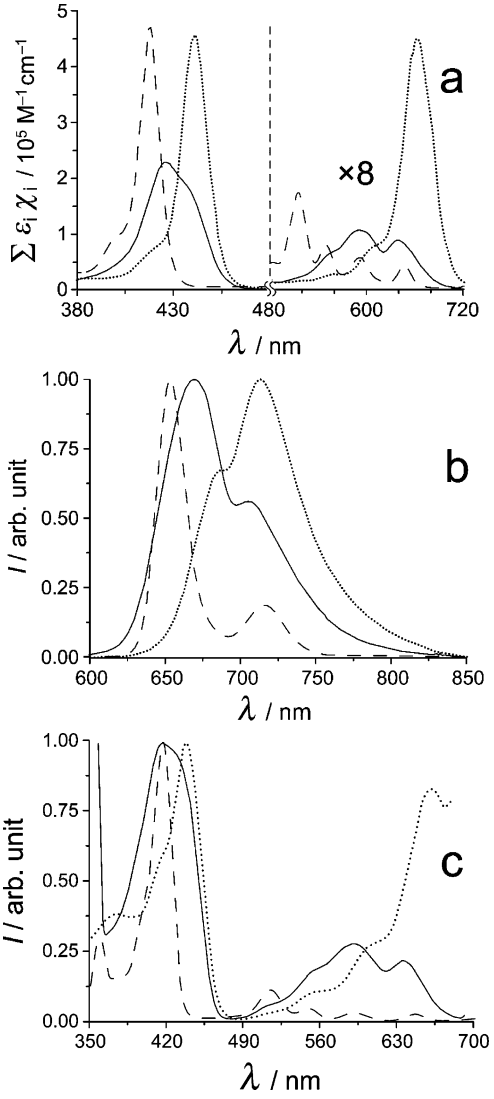

Figure 2. Absorption (a), normalized fluorescence emission (b), and excitation (c) spectra of *DA* (dotted line), *MA* (solid line), and *FB* (dashed line) derivatives for the H_2TPP/HTFPB system. (UV/vis spectra normalized with respect to optical path length and total porphyrin concentration.) (b) Excitation wavelengths: 454 nm (*DA*), 451 nm (*MA*), and 428 nm (*FB*). (c) Emission wavelengths: 709 nm (*DA*), 707 nm (*MA*), and 716 nm (*FB*).

Results and Discussion

Spectroscopic Studies. The addition of tetrakis[3,5-bis-(trifluoromethyl)phenyl]boric acid (HTFPB) to a purple solution of H_2TPP in dichloromethane causes a change to a deep emerald green. The absorption spectrum of the strongly acidic solution displays a sharp Soret band centered at 441 nm and three Q-bands at 558, 609, and 662 nm, with a profile

(39) Perdew, J. P. *Phys. Rev. B: Condens. Matter* **1986**, *33*, 8822−8824 (Erratum: PRB 8834 (1986) 7406).
(40) Becke, A. D. *Phys. Rev. A* **1988**, *38*, 3098−3100.
(41) Gross, E. K. U.; Kohn, W. *Adv. Quantum Chem.* **1990**, *21*, 255.
(42) Gross, E. K. U.; Dobson, J. F.; Petersilka, M. In *Density Functional Theory, Springer Series "Topics in Current Chemistry"*; Nalewajski, R. F., Ed.; Springer: Heidelberg, 1996.
(43) Casida, M. E. In *Recent Advances in Density Functional Methods*; Chong, D. P., Ed.; World Scientific: Singapore, 1995; Vol. 1, p 155.
(44) Bauernschmitt, R.; Ahlrichs, R. *J. Chem. Phys.* **1996**, *104*, 9047.
(45) Bauernschmitt, R.; Ahlrichs, R. *Chem. Phys. Lett.* **1996**, *256*, 454.
(46) Bauernschmitt, R.; Häser, M.; Treutler, O.; Ahlrichs, R. *Chem. Phys. Lett.* **1997**, *264*, 573.
(47) Gritsenko, O. V.; Schipper, P. R. T.; Baerends, E. J. *Chem. Phys. Lett.* **1999**, *302*, 199.
(48) Schipper, P. R. T.; Gritsenko, O. V.; van Gisbergen, S. J. A.; Baerends, E. J. *J. Chem. Phys.* **2000**, *112*, 1344.
(49) Lee, C.; Yang, W.; Parr, R. G. *Phys. Rev. B* **1988**, *37*, 785.
(50) Becke, A. D. *J. Chem. Phys.* **1993**, *98*, 5648.
(51) Amsterdam Density Functional Program; Theoretical Chemistry, Vrije Universiteit: Amsterdam, The Netherlands. htpp://www.scm.com (accessed month year).
(52) te Velde, G.; Bickelhaupt, F. M.; Baerends, E. J.; Fonseca Guerra, C.; van Gisbergen, S. J. A.; Snijders, J. G.; Ziegler, T. *J. Comput. Chem.* **2001**, *22*, 931−967.
(53) Ahlrichs, R.; Bär, M.; Häser, M.; Horn, H.; Kölmel, C. *Chem. Phys. Lett.* **1989**, *162*, 165.
(54) Schäfer, A.; Horn, H.; Ahlrichs, R. *J. Chem. Phys.* **1992**, *97*, 2571.
(55) Dunning, T. H., Jr. *J. Chem. Phys.* **1989**, *90*, 1007−1023.

Table 1. UV/vis Absorption, Emission, and Photophysical Parameters of H_2TPP Porphyrin and the Relative Protonated Forms in the Presence of the Various HX in Dichloromethane at 298 K

species	B-band	Q-bands	emission	Φ_f[a]	τ_f/ns (%)[b]
H_2TPP	418	515; 549; 592; 646	651; 716	0.10	8.40
$\{H_3TPP(TFPB)\}$	424; 440	552; 580; 603; 636; 657	668; 708	0.07	1.13 (0.42); 1.9 (0.58)
$\{H_4TPP(TFPB)_2\}$	441	609; 662	683; 709	0.11	2.45 (0.91); 0.1 (0.09)
$\{H_4TPP(PF_6)_2\}$	438	606; 659	685; 713		
$\{H_4TPP(Cl)_2\}$	446	613; 665	682; 703	0.10	2.24

[a] Relative to TPP in nondegassed benzene ($\Phi = 0.11$).[83] [b] Nondegassed samples.

typical of H_2TPP diacid derivatives.[2,3,7,8,18] Upon dilution of solutions containing this species, characterized as the diacid $\{H_4TPP(TFPB)_2\}$,[56] complex changes in the absorption profile have been observed, pointing to the occurrence of multiple equilibria in solution (Figure 1). Indeed, the UV/vis spectral changes relative to stepwise acidification of a dilute H_2TPP solution with HTFPB, or dilution of a concentrated $\{H_4TPP(TFPB)_2\}$ solution with neat CH_2Cl_2, indicate the presence of three species with well different optical properties (Figure 2). Since no aggregation has been detected via resonance light scattering measurements at the porphyrin concentration used in the experiments (total H_2-TPP concentration: from 5.10×10^{-4} M to 2×10^{-7} M), this evidence has been tentatively attributed to the conversion of the diacid species (*DA*) into its free base form (*FB*) through the formation of a well distinct porphyrin monoprotonated at the core ($\{H_3TPP(TFPB)\}$; *MA*). The broad and asymmetric *MA* Soret band consists of multiple components, the two main absorption features being centered at 424 and 440 nm (Figure 2a).

The difference in the Q-band profiles of *FB*, *MA*, and *DA* is worth noting. Though only few cases are reported on the formation of *meso*-aryl monoacid porphyrins, Q-band patterns similar to that of *MA* have been previously attributed to monoprotonated porphyrin macrocycles.[9,17,18,21,25,57,58] Quite interestingly, a similar pattern has also been reported for triarylcorroles, that possess three central pyrrole N−H groups and are neutral.[59,60]

The fluorescence emission spectra of the *FB* species exhibit a typical two-banded feature, which undergoes a progressive red-shift upon protonation to the *MA* and the *DA* (Figure 2b and Table 1). The emission profiles of the three species are found to be independent of the excitation wavelength (see 3D fluorescence experiments, Figures SI2 and SI3, Supporting Information),[61] pointing to the presence of isolated fluorophores in the corresponding solutions. In agreement with this conclusion, also the excitation spectra recorded for the three species match the corresponding absorption spectra, regardless of the emission wavelength chosen for the observation (Figure 2c). The *FB* porphyrin shows a fluorescence decay which can be well described by a monoexponential curve with a $\tau = 8.4$ ns. For the *DA* species, the decay profile can be fitted to a double-exponential model, with a longer lifetime of 2.45 ns which accounts for 91% of the relative amplitude and a shorter one of 0.1 ns, exhibiting a smaller amplitude (9%). These results together with the relative fluorescence quantum yields measured on *FB* and *DA* species are well in agreement with the literature data.[33,62] The fluorescence emission of *MA* species evidences a double exponential decay with almost equally distributed lifetimes of 1.9 (58%) and 1.13 (42%) ns. These data, the relatively high value for the fluorescence quantum yield ($\Phi_f = 0.07$) and the previously cited RLS experiments, suggest the absence of aggregates and point to the monomeric nature of this species.

Since no intermediate species were detected in the acidification experiments previously carried out on H_2TPP with various HX,[7,15,22,24,33,63] we thought that the formation of the elusive *MA* was possibly related to the large and noncoordinating $TFPB^-$ anion. To verify this hypothesis dilution experiments were performed as a function of the anion, by starting from diacid derivatives having PF_6^- and Cl^- as counteranions. On diluting a concentrated $\{H_4TPP(PF_6)_2\}$ solution, the absorption spectrum of the diacid derivative converts to that of the free base without isosbestic points in the corresponding UV/vis spectral changes (Figure SI4), indicating the formation of an intermediate species also in this case, even if the interconversion is less clear (Figure 3a). The main component of *MA* Soret band is approximately centered at 425 nm, and three Q-bands can be identified around 556, 593, and 643 nm. The corresponding fluorescence spectrum (Figure 3b) displays a two-banded emission (672, 706 nm) with a profile similar to that of $\{H_3TPP(TFPB)\}$.[64] A completely different pattern of behavior is exhibited by the chloride system, which shows anyway the

(56) Simplified symbol for $\{(H_2TPP^{2+})\cdot(TFPB^-)_2\}$. Hereafter, this notation will be used to represent ion pairs, unless otherwise specified.

(57) Neuberger, A.; Scott, J. J. *Proc. R. Soc. London, Ser. A* **1952**, *A213*, 307−326.
(58) Corwin, A. H.; Chivvis, A. B.; Poor, R. W.; Whitten, D. G.; Baker, E. W. *J. Am. Chem. Soc.* **1968**, *90*, 6577−6583.
(59) Gross, Z.; Galili, N.; Saltsman, I. *Angew. Chem., Int. Ed.* **1999**, *38*, 1427−1429.
(60) Mahammed, A.; Weaver, J. J.; Gray, H. B.; Abdelas, M.; Gross, Z. *Tetrahedron Lett.* **2003**, *44*, 2077−2079.
(61) This evidence also confirms that the 440 nm band is not due to a residual amount of *DA*.
(62) Chirvony, V. S.; van Hoek, A.; Galievsky, V. A.; Sazanovich, I. V.; Schaafsma, T. J.; Holten, D. *J. Phys. Chem. B* **2000**, *104*, 9909−9917.
(63) Knyukshto, V. N.; Solovyov, K. N.; Egorova, G. D. *Biospectroscopy* **1998**, *4*, 121−133.
(64) It has never been possible to separate $\{H_3TPP(PF_6)\}$ from the corresponding *DA* or from the *FB*: the absorption spectra of the solutions mainly containing this *MA* always have shown contributions from either one or the other species. This conclusion has also been confirmed by recording the corresponding emission spectra, whose profiles have presented a dependence on the excitation wavelength in agreement with the simultaneous presence of more than one species in the *MA* solution. For this reason, the deconvolution of the *MA* absorbance spectrum has not been attempted, nor the photophysical properties of this species have been measured.

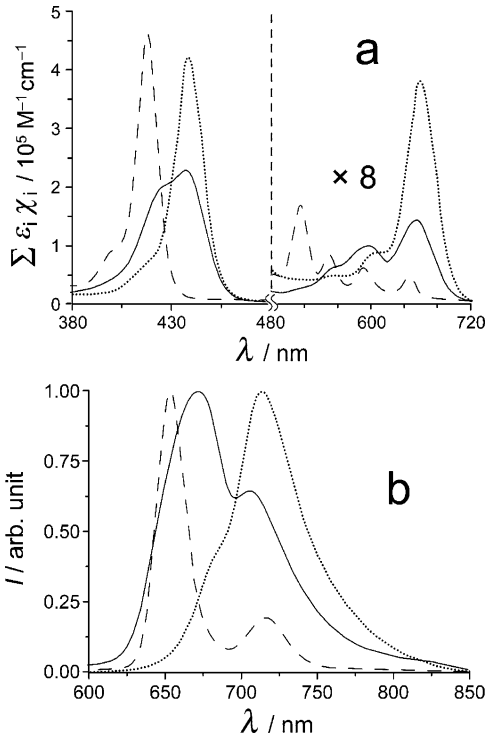

Figure 3. Absorption (a) and normalized fluorescence emission (b) spectra of $\{H_4TPP(PF_6)_2\}$ (*DA*, dotted line), $\{H_3TPP(PF_6)\}$ (*MA*, solid line), and H_2TPP (*FB*, dashed line). (a) Normalized spectra. (b) Excitation wavelengths: 456 nm (*DA*), 424 nm (*MA*), and 410 nm (*FB*).[66]

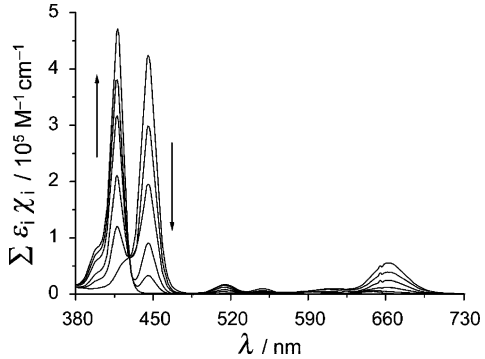

Figure 4. UV/vis spectral changes upon dilution of a dichloromethane solution of $\{H_4TPP(Cl)_2\}$. Total H_2TPP concentration: from 4.38×10^{-4} M to 6.4×10^{-6} M. Spectra have been normalized with respect to optical path length and total concentration (see the Experimental Section).

presence of an equilibrium between $\{H_4TPP(Cl)_2\}$ and H_2-TPP, but no evidence of intermediate species (Figure 4).[65]

Theoretical Studies. To provide further support to the assignment of the intermediate species spectroscopically detected in solution, we have theoretically investigated the ground state molecular and electronic structure and the optical spectra of *MA* and *DA* having PF_6^- as counterion.

(a) Molecular Structure. Unconstrained geometry optimization of $\{H_4TPP(PF_6)_2\}$ afforded the C_1 symmetry structure displayed in Figure 5. Similar to other H_2TPP diacids,[2,32,67] $\{H_4TPP(PF_6)_2\}$ exhibits a pronounced saddling

(65) The same observation has been reported for the TPP/HCl system in dimethyl sulfoxide−water. See ref 24.
(66) The absorption spectrum of *MA* shows some contributions from *DA*.
(67) Senge, M. O.; Kalisch, W. W. *Z. Naturforsch. B: Chem. Sci.* **1999**, *54b*, 943.

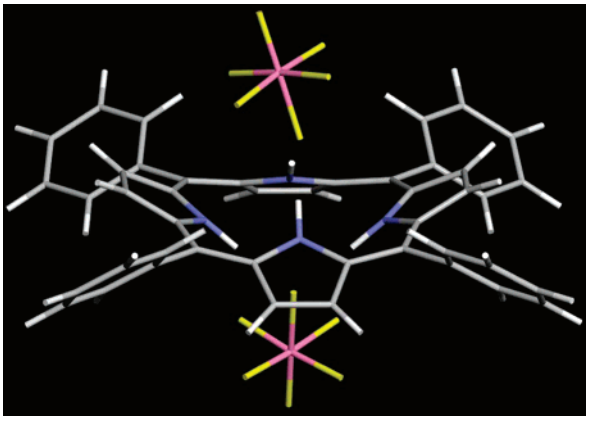

Figure 5. DFT-calculated structure of $\{H_4TPP(PF_6)_2\}$.

of the porphyrin core (average φ[68] = 27.8°) and a considerable tilting of the *meso*-phenyl rings (average θ[69] = 37.3°). Nearly linear hydrogen bonds bridge one fluorine atom of each PF_6^- unit and a cofacial pair of trans pyrrole NH protons, with the N−H···F bond angle and the N···F distance averaging 176° and 2.80 Å, respectively. The calculated N···F distances are ca. 0.2 Å shorter than those observed in hydrogen-bonded adducts of cationic transition metal complexes with PF_6^- anions.[70,71] The two PF_6^- units show a pseudo-octahedral geometry with the distance between P and the fluorine atom engaged in the hydrogen bonding interaction being significantly longer than the other P−F distances (1.77 vs 1.62 Å in the average). Structures with two *cis*-fluorine atoms of each PF_6^- unit pointing to the cofacial pair of trans pyrrole N−H groups were also theoretically explored for $\{H_4TPP(PF_6)_2\}$. However, they invariably converged to the C_1 structure of Figure 5.

As for the monoacid species, $\{H_3TPP(PF_6)\}$, several structures corresponding to different conformations of the porphyrin core and orientations of the anion have been theoretically explored. Two stable, nearly degenerate isomers were found in our extensive search for stationary points, their structures being displayed in Figure 6.

The lowest energy isomer, **a**, has C_s symmetry, and it can be considered as derived from $\{H_4TPP(PF_6)_2\}$ by removing one PF_6^- anion and one of the bonded NH protons. Due to the loss of a central proton, *MA* is significantly less saddled (average φ = 21.5°) than *DA*. The tilting angle of the *meso*-phenyl rings, θ, is in *MA* larger than in the parent diacid (44.5° vs 37.3°). This is consistent with experimental data[32,72,73] and recent theoretical studies[74] showing that a smaller degree of saddling correlates with less acute porphyrin-aryl dihedral angles. The calculated hydrogen bond parameters are substantially the same as in *DA*, with the

(68) The angle that a pyrrole ring makes with the porphyrin plane.
(69) The angle between the phenyl plane and the porphyrin plane.
(70) Akashi, H.; Yamauchi, T.; Shibahara, T. *Inorg. Chim. Acta* **2004**, *357*, 325.
(71) Braga, D.; Giaffreda, S. L.; Polito, M.; Grepioni, F. *Eur. J. Inorg. Chem.* **2005**, 2737.
(72) Scheidt, W. R.; Lee, Y. J. *Struct. Bonding* **1987**, *64*, 1.
(73) Munro, O. Q.; Bradley, J. C.; Hancock, R. D.; Marques, H. M.; Marsicano, F.; Wade, P. W. *J. Am. Chem. Soc.* **1992**, *114*, 7218.
(74) Rosa, A.; Ricciardi, G.; Baerends, E. J. *J. Phys. Chem. A* **2006**, *110*, 5180−5190.

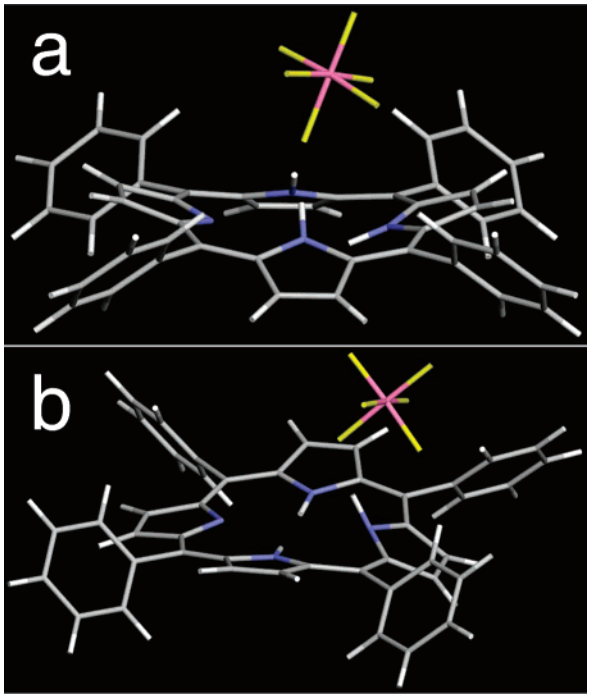

Figure 6. DFT-calculated structures of $\{H_3TPP(PF_6)\}$.

N−H···F bond angle and the N···F distance being 175° and 2.81 Å, respectively.

The **b** isomer, which is only 1.3 kJ/mol higher in energy, possesses C_1 symmetry and differs significantly from the **a** isomer in either the conformation of the porphyrin core and the H_3TPP^+/PF_6^- interaction mode. Three of the four pyrroles are modestly saddled, with the interplanar angle between adjacent pyrrole rings averaging 10°. The fourth pyrrole ring, the one involved in hydrogen bonding with one fluorine atom of the PF_6^- anion, is significantly tilted out of the mean porphyrin plane, with the interplanar angle between this pyrrole ring and the adjacent ones averaging 20°. The NH proton of this pyrrole is displaced ca. 0.6 Å from the pyrrole plane, that is indicative of appreciable sp^3 hybridization of the nitrogen atom. Most likely such hybridization guarantees a strong hydrogen bonding interaction with the PF_6^- unit while avoiding steric hindrance between the monocation and the bulky counterion. As a matter of fact, in **b** the N···F distance is shorter and the N−H···F bond angle is more acute than in **a** (2.69 Å vs 2.81 Å, 165° vs 175°).

Interestingly, the conformation adopted by the porphyrin core in the **b** isomer closely resembles that observed in the structurally characterized octaethylporphyrin monoacid $\{H_3OEP(X)\}$ ($X = I_3$, $Re_2(CO)_6Cl_3$).[75,76] In these salts, the H_3OEP^+ monocation exhibits three nearly coplanar pyrrole rings with the plane of the fourth ring tilted significantly (8.6−14°) from the mean plane of the other three. It is worthwhile to note that the structure of the **b** isomer is also very similar to that reported by Gross et al.[77] for a triarylcorrole. This latter is a neutral tetrapyrrole macrocycle with three N−H groups, exhibiting a remarkable out of pyrrole plane location of one of these NH bonds. This structural feature is dictated by the necessity to minimize the steric hindrance between the inner protons, which is particularly large due to the contracted central cavity of corroles.

Although the **a** isomer is the most stable in the gas phase, the small energy gap (∼RT at room temperature) between **a** and **b** isomers should make them both accessible in solution. Therefore, for completeness, it is deemed necessary to consider the optical spectrum of both isomers.

(b) Optical Spectra. TDDFT calculations have been performed for $\{H_4TPP(PF_6)_2\}$ and the two $\{H_3TPP(PF_6)\}$ isomers using both pure (BP86 and SAOP) and hybrid (B3LYP) functionals, to provide an assignment of the salient features of the electronic absorption spectra of the diacid and the supposed monoacid species. The excitation energies and oscillator strengths calculated for the lowest optically allowed excited states are gathered in Tables 2−4 together with the major one-electron transitions contributing to the excited-state solution vectors. The energy and labeling of the Kohn−Sham MOs involved in the one-electron transitions are indicated in the level scheme of Figure 7.

The TDDFT results for $[H_4TPP](PF_6)_2$ are discussed first. As inferred from the data in Table 2, the two lowest, nearly degenerate 1^1A and 2^1A excited states nicely account for the quite intense Q-band appearing at 659 nm in the spectrum of $\{H_4TPP(PF_6)_2\}$. The lifting of the near degeneracy of the highest occupied Gouterman MOs (see level scheme of Figure 7), due to the phenyl tilting induced upshift of the "a_{2u}"-HOMO,[8,74] causes the "a_{1u}"→ "e_g" and "a_{2u}"→ "e_g" Gouterman transitions to mix very little. Accordingly, the 1^1A and 2^1A excited states are dominated by the "a_{2u}" (231a) → "e_g" (232a, 233a) transition, the "a_{1u}" (231a) → "e_g" (232a, 233a) entering only with a minor weight (20−23%). Due to the reduced mixing of the Gouterman configurations, the cancellation of their large transition dipoles is less effective than in the parent free base,[8] leading, in fairly good agreement with the experiment (see Figure 2a), to an intensification of the Q-band for which we compute a summed oscillator strength of ca. 0.3. No additional excited states are predicted in the Q-band region suggesting that the weak features appearing to the blue of the lowest-energy Q-band are vibrational in origin, as in the $\{H_4TPP(X)_2\}$ (X = F, Cl, Br, I) series.[8]

Concerning the B band centered at 438 nm, TDDFT/B3LYP calculations assign it to the next pair of nearly degenerate excited states (3^1A and 4^1A calculated at 408 nm with summed oscillator strength of 2.6). These states are dominated by the "a_{1u}" (230a) → "e_g" (232a, 233a) transition, the lower-energy Gouterman transition, the "a_{2u}" (231a) → "e_g" (232a, 233a), entering with a minor weight (22%). Even better agreement with the experiment is obtained at the BP86 and the SAOP levels, the pair of states responsible for the intensity of the B band, the 4^1A and 5^1A, being calculated at 451 and 449 nm, respectively. At variance with B3LYP the pure functionals describe the excited states accounting for the B band as a mixture of the Gouterman transitions and higher energy $\pi\rightarrow\pi^*$ transitions and predict in the B

(75) Hirayama, N.; Takenaka, A.; Sasada, Y.; Watanabe, E.; Ogoshi, H.; Yoshida, Z. *J. Chem. Soc., Chem. Commun.* **1974**, 330−331.
(76) Hrung, C. P. *J. Am. Chem. Soc.* **1978**, *100*, 6068−6076.
(77) Gross, Z.; Galili, N.; Simkhovich, L.; Saltsman, I.; Botoshansky, M.; Bläser, D.; Boese, R.; Goldberg, I. *Org. Lett.* **1999**, *1*, 599−602.

Table 2. Composition, Vertical Excitation Energies, *E*/nm, and Oscillator Strengths, *f*, Computed for the Lowest Optically Allowed Excited States of $\{H_4TPP(PF_6)_2\}$ at Various Levels of Theory

	TDDFT/BP86			TDDFT/SAOP			TDDFT/B3LYP			
state	composition (%)	*E*	*f*	composition (%)	*E*	*f*	composition (%)	*E*	*f*	exp (nm)
1^1A	77 (231a → 233a, 232a)	671	0.145	76 (231a → 233a, 232a)	669	0.136	77 (231a → 233a, 232a)	627	0.167	659 Q
	22 (230a → 232a, 233a)			23 (230a → 232a, 233a)			23 (230a → 232a, 233a)			
2^1A	77 (231a → 232a, 233a)	671	0.153	76 (231a → 232a, 233a)	669	0.137	77 (231a → 232a, 233a)	626	0.167	
	21 (230a → 233a, 232a)			23 (230a → 233a, 232a)			23 (230a → 233a, 232a)			
3^1A	41 (231a → 234a)	454	0.112	36 (231a → 234a)	453	0.174	71 (230a → 232a)	408	1.23	438 B
	25 (228a → 233a)			24 (228a → 233a)			21 (231a → 233a)			
	9 (230a → 233a)			12 (230a → 233a)						
4^1A	46 (230a → 232a)	451	0.512	45 (230a → 232a)	451	0.562	72 (230a → 233a)	408	1.23	
	16 (228a → 232a)			13 (231a → 233a)			21 (231a → 232a)			
	11 (231a → 233a)			12 (228a → 232a)						
5^1A	37 (230a → 233a)	449	0.401	34 (230a → 233a)	449	0.398				
	16 (229a → 232a)			17 (229a → 232a)						
	8 (231a → 232a)			12 (231a → 232a)						

Table 3. Composition, Vertical Excitation Energies, *E*/nm, and Oscillator Strengths, *f*, Computed for the Lowest Optically Allowed Excited States of $\{H_3TPP(PF_6)\}$ **a** at Various Levels of Theory

	TDDFT/BP86			TDDFT/SAOP			TDDFT/B3LYP			
state	composition (%)	*E*	*f*	composition (%)	*E*	*f*	composition (%)	*E*	*f*	exp (nm)
$1^1A''$	73 (107a′ → 90a″)	656	0.069	71 (107a′ → 90a″)	654	0.061	71 (107a′ → 90a″)	615	0.071	643 Q
	26 (89a″ → 108a′)			28 (89a″ → 108a′)			28 (89a″ → 108a′)			
$1^1A'$	76 (107a′ → 108a′)	642	0.134	74 (107a′ → 108a′)	640	0.118	75 (107a′ → 108a′)	598	0.142	
	23 (89a″ → 90a″)			24 (89a″ → 90a″)			24 (89a″ → 90a″)			
$2^1A'$	97 (106a′ → 108a′)	497	∼0	97 (106a′ → 108a′)	481	∼0	89 (106a′ → 108a′)	406	0.047	425, 440[a] B
$2^1A''$	92 (106a′ → 90a″)	494	0.006	89 (106a′ → 90a″)	478	0.024	52 (106a′ → 90a″)	422	0.376	
	6 (89a″ → 108a′)			8 (89a″ → 108a′)			35 (89a″ → 108a′)			
							10 (107a′ → 90a″)			
$3^1A''$	55 (105a′ → 90a″)	454	0.303	38 (89a″ → 108a′)	443	0.699	43 (106a′ → 90a″)	395	0.930	
	26 (89a″ → 108a′)			16 (107a′ → 90a″)			30 (89a″ → 108a′)			
	10 (107a′ → 90a″)			15 (105a′ → 90a″)			15 (107a′ → 90a″)			
$3^1A'$	67 (105a′ → 108a′)	446	0.149	55 (89a″ → 90a″)	440	0.670	65 (89a″ → 90a″)	398	1.17	
	22 (89a″ → 90a″)			16 (107a′ → 108a′)			20 (107a′ → 108a′)			
	6 (107a′ → 108a″)									
$4^1A'$	35 (89a″ → 90a′)	433	0.595							
	30 (105a′ → 108a″)									
	10 (107a′ → 108a″)									
$5^1A''$	35 (105a′ → 90a″)	427	0.697							
	30 (89a″ → 108a′)									
	10 (107a′ → 90a″)									

[a] Observed in the absorption spectrum of $\{H_3TPP(TFPB)\}$.

Table 4. Composition, Vertical Excitation Energies, *E*/nm, and Oscillator Strengths, *f*, Computed for the Lowest Optically Allowed Excited States of $\{H_3TPP(PF_6)\}$ (**b**) at Various Levels of Theory

	TDDFT/BP86			TDDFT/SAOP			TDDFT/B3LYP			
state	composition (%)	*E*	*f*	composition (%)	*E*	*f*	composition (%)	*E*	*f*	exp (nm)
1^1A	72 (196a → 197a)	635	0.077	70 (196a → 197a)	633	0.070	70 (196a → 197a)	597	0.084	643 Q
	26 (195a → 198a)			28 (195a → 198a)			28 (195a → 198a)			
2^1A	69 (196a → 198a)	619	0.068	67 (196a → 198a)	600	0.059	67 (196a → 198a)	578	0.072	
	29 (195a → 197a)			31 (195a → 197a)			31 (195a → 197a)			
3^1A	93 (194a → 197a)	472	0.002	92 (194a → 197a)	461	0.010	48 (194a → 197a)	406	0.413	425, 440[a] B
							35 (195a → 198a)			
							10 (196a → 197a)			
4^1A	95 (194a → 198a)	460	0.005	92 (194a → 198a)	449	0.017	61 (195a → 197a)	396	1.310	
							28 (196a → 198a)			
5^1A	32 (193a → 197a)	441	0.406	29 (195a → 198a)	440	0.470	48 (194a → 197a)	388	0.874	
	23 (195a → 198a)			23 (193a → 197a)			29 (195a → 198a)			
	8 (196a → 197a)			11 (196a → 197a)			15 (196a → 197a)			
6^1A	31 (195a → 197a)	440	0.526	39 (195a → 197a)	438	0.627	96 (194a → 198a)	376	0.030	
	11 (196a → 198a)			15 (196a → 198a)						
	8 (193a → 198a)									

[a] Observed in the absorption spectrum of $\{H_3TPP(TFPB)\}$.

band region a third, rather weak excited state (3^1A) mainly described by non-Gouterman transitions.

We come now to the theoretical interpretation of the optical spectra of the monoacid species. To simplify the arguments, we first concentrate on the theoretical results obtained for the most stable C_s structure of $\{H_3TPP(PF_6)\}$ and later point out the effects of the **a** → **b** structural change.

As inferred from the TDDFT results in Table 3, only two close-lying excited states are calculated in the energy regime of the Q-bands ($1^1A''$ and $1^1A'$). These states are largely

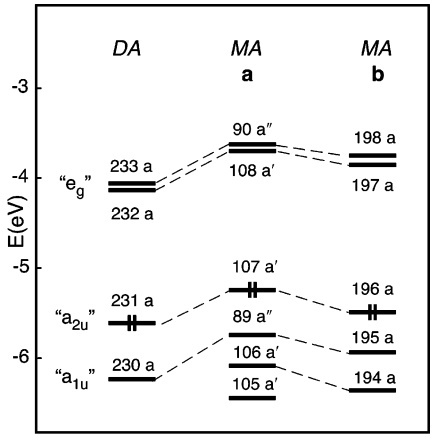

Figure 7. Energy level scheme for {$H_4TPP(PF_6)_2$} and the {$H_3TPP(PF_6)$} **a** and **b** isomers obtained at the BP86 level. For the Gouterman MOs the formal D_{4h} notation is also reported in inverted commas.

described by the "a_{2u}" (107a′) → "e_g" (90a″, 108a′) transition, while the "a_{1u}" (89a″) → "e_g" (108a′, 90a″) enters with only a minor weight. They can be considered as the best candidates for assignment to the longest-wavelength Q-band centered at ca. 643 nm in the optical spectrum of the monoacid species. The energy of this band is indeed well reproduced theoretically, particularly at the SAOP and the BP86 levels. The observed blue shift and hypochromicity of the Q-band going from *DA* to *MA* species is fully accounted for by the excitation energies and oscillator strengths calculated for the $1^1A''/1^1A'$ pair of states. The blue shift of the long wavelength Q-band moving from *DA* to *MA* is also consistent with the increase of the HOMO/LUMOs gap (cf. the level scheme of Figure 7), which is due to the less pronounced destabilization of the HOMO consequent to the reduced degree of tilting of the phenyl rings. In turn, the reduced intensity of the Q-band on going from *DA* to *MA* is in line with the reduced HOMO/HOMO-1 gap, that causes a somewhat larger mixing of the Gouterman transitions and hence a more effective cancellation of their large transition dipole moments. TDDFT results clearly point to the vibrational character of the features appearing to the blue of the longest-wavelength Q-band, which is also consistent with the observed shift to the blue of the whole Q-band system upon dilution of the diacid solution.

The theoretical description of the B band region is complicated by the presence of non-Gouterman transitions from the two pyrrolenine MOs—the 106a′ and 105a′ displayed in Figure 8—to the unoccupied Gouterman MOs. These transitions have some charge transfer (CT) character as they involve excitation of one electron from MOs localized on one pyrrole ring into MOs delocalized over all four pyrrole rings.[78] As TDDFT methods tend to underestimate the energy of CT transitions,[79,80] they are likely to be calculated at somewhat too low an energy. As a matter of fact, they either appear as very weak extra bands to the red of Soret band—this is the case of the $2^1A'$ and $2^1A''$ pair of states (BP86 and SAOP) or the $2^1A'$ (B3LYP)—or undergo configuration mixing with the Gouterman transitions. The extent to which this mixing occurs depends on the energy of the involved MOs and hence varies on changing the exchange-correlation functional. At the BP86 level the Gouterman transitions heavily mix with the 105a′ → 90a″, 108a′ CT transitions. Four excited states are generated, the most intense of which, the $4^1A'$ and $5^1A''$, are dominated by the Gouterman transitions. The $5^1A''$ state computed at 427 nm with an oscillator strength of 0.697 well accounts for the main component of the Soret band appearing at ca. 425 nm in the optical spectra of both {$H_3TPP(PF_6)$} and {H_3-TPP(TFPB)} monoacid species. In turn, the $4^1A'$ state at 433 nm with an oscillator strength of 0.595 accounts for the red component of the B band, which is clearly detectable in the optical spectrum of {$H_3TPP(TFPB)$}, at around 440 nm. At the SAOP level the mixing of the Gouterman transitions with the CT transitions is virtually absent. Indeed, of the two excited states accounting for the intensity of the B band features, the $3^1A''$ and $3^1A'$, only the former is contaminated to some extent (15%) by the 105a′ → 90a″ CT transition (cf. Table 3). At the B3LYP level the 105a′ → 90a″, 108a′ CT transitions are too high in energy to mix with the Gouterman transitions. It is rather the 106a′ → 90a″ that heavily mixes with the Gouterman transitions in the $2^1A''$

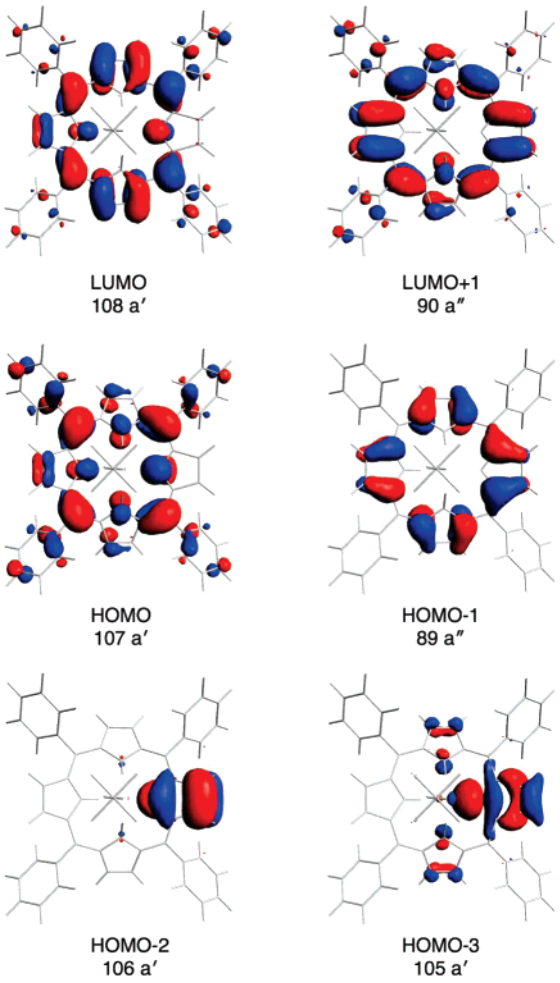

Figure 8. Frontier molecular orbitals for the {$H_3TPP(PF_6)$} **a** isomer.

(78) Cai, Z.-L.; Crossley, M. J.; Reimers, J. R.; Kobayashi, R.; Amos, R. D. *J. Phys. Chem. B* **2006**, *110*, 15624.
(79) Dreuw, A.; Head-Gordon, M. *J. Am. Chem. Soc.* **2004**, *126*, 4007.
(80) Gritsenko, O.; Baerends, E. J. *J. Chem. Phys.* **2004**, *112*, 655.

and $3^1A''$ excited states, the intense $3^1A'$ at 398 nm being a "pure" B state. When we isolate spectral features predictions that are consistent across all methods, it becomes clear that in the energy regime of the broad and asymmetric B band both pure and hybrid functionals locate two intense close-lying excited states, the $4^1A'/5^1A''$ pair according to the BP86 results and the $3^1A'/3^1A''$ pair at the SAOP and the B3LYP level. The energies and intensities calculated for these states leave little doubt on their assignment to the main features of the B band of the monoacid species. Notably, the blue shift of the Soret band of *MA* relative to *DA* is also faithfully reproduced theoretically.

TDDFT results for the **b** structure of $\{H_3TPP(PF_6)\}$ proved to be quite similar to those obtained for the **a** structure. As it can be inferred from the energies and oscillator strengths calculated for the two lowest excited states accounting for the Q-band (1^1A and 2^1A), the **a** → **b** structural change results in a modest blue shift and weakening of this band (Table 4). This is consistent with (i) the increased gap between the HOMO (196a) and the two nearly degenerate unoccupied Gouterman MOs (197a, 198a) and (ii) the diminished HOMO−HOMO-1 energy gap (cf. the level scheme of Figure 7).

Concerning the B band region, both BP86 and SAOP predict four excited states. However, the lowest two, the very weak 3^1A and 4^1A, have a pure CT character as they involve transitions from the higher lying pyrrolenine MO, the 194a (see Figures 7 and 8), to the empty Gouterman MOs, the 197a and 198a. Therefore, they are artificially located between the Q- and B-bands. The next two states, the quite intense 5^1A and 6^1A, are mainly composed of the Gouterman transitions, with minor contributions from CT transitions involving occupied π-phenyl orbitals (e.g., the 193a) and the empty Gouterman MOs, so their calculated energies are trustable. The energies and oscillator strengths computed for these states satisfactorily account for the B band of the monoacid species. At the B3LYP level the Gouterman transitions heavily mix with the 194a → 197a CT transition. Three close-lying excited states arise from this configuration mixing, the moderately intense 3^1A at 406 nm, and the very intense 4^1A and 5^1A, at 396 and 388 nm, respectively. These states provide a reasonably good description of the B band region.

Altogether the TDFFT results for the **a** and **b** isomers of $\{H_3TPP(PF_6)\}$ strongly support the assignment of the spectral features of the intermediate species identified during the dilution experiments to a monoacid species. As both isomers reproduce the main spectral features of the monoacid species, it is hard to say which of the two structures is actually adopted by $\{H_3TPP(PF_6)\}$ in solution. Incidentally we note that the *MA* spectrum closely resembles that of triarylcorroles,[77] whose structure is very similar to that of the **b** isomer.

(C) Role of the Counteranions in the Stabilization of the MA Species. When comparing the dilution experiments for the three *DA* species, it can be noted that the range of concentration in which *MA* is the most abundant one narrows going from $\{H_4TPP(TFPB)_2\}$ to $\{H_4TPP(PF_6)_2\}$, the *MA* species being completely absent for the chloride derivative.

Table 5. Enthalpies (ΔH, kJ mol^{-1}), Entropies (ΔS, kJ mol^{-1} K^{-1}), Gibbs Free Energies (ΔG, kJ mol^{-1}), and Equilibrium Constants (K_i) Calculated in the Gas Phase for the Dissociation Equilibria **1** and **2** in the Case of Cl^- as Counteranion[a]

eq	ΔH	ΔS	ΔG	K
1	115.6	0.1641	66.7	2.0×10^{-12}
2	48.4	0.1672	−1.5	1.8

[a] $T = 298.15$ K, $P = 1$ atm.

Intuitively, this suggests that the nature of the anion largely influences the relative values of the equilibrium constants for the two dissociation steps

$$\{(H_4TPP^{2+})\cdot(X^-)_2\} \overset{K_2}{\rightleftharpoons} \{(H_3TPP^+)\cdot(X^-)\} + HX \quad (1)$$

$$\{(H_3TPP^+)\cdot(X^-)\} \overset{K_1}{\rightleftharpoons} H_2TPP + HX \quad (2)$$

In particular, to account for our experimental evidence, K_2 should be larger than K_1 for $TFPB^-$ and PF_6^-, while this trend should be reversed for Cl^-.[81] In order to get a deeper insight on this issue, we performed an analysis on the magnitude of K_2 and K_1 through thermodynamic calculations in the gas phase. The calculations were only performed for X = Cl, because of the difficulty to properly model the molecular structure of HPF_6 in the gas phase, in the absence of structural information on this species either in gas phase and in organic solvent solution. In the gas phase, the Gibbs free energy of each species involved in the reaction is related to its enthalpy by

$$G_{gas} = H_{gas}(T) - TS_{gas}^{trans} - TS_{gas}^{rot} - TS_{gas}^{vib}$$

The part $H(T)$ contains the internal potential energy of the ideal gas and the standard contributions due to the zero-point temperature corrections and the finite temperature corrections to the enthalpy. The entropic terms for translational, rotational, and vibrational motion are obtained from standard expressions.[82] The gas-phase enthalpies, entropies, Gibbs free energies, and equilibrium constants computed for the dissociation equilibria 1 and 2 at 298.15 K are reported in Table 5. The obtained values support the predicted trend for the relative values of the equilibrium constants, indicating that the conversion from *DA* to *MA* for Cl^- is unfavorable due to a largely positive ΔH term. The loss of the second HCl molecule is still endothermic, but the Gibbs free energy change is slightly negative, making this step more favored with respect to the former. The low K_2/K_1 ratio is in line with the experimental difficulty of detecting the *MA* species with Cl^-.

The observed experimental trend for the stabilization of MA intermediate species ($TFPB^- > PF_6^- > Cl^-$) could be ascribed to an interplay of different properties of the

(81) Due to the high volatility of the solvent and to the limited number of data points, the determination of the values of the equilibrium constants is rather unreliable. A rough estimate for PF_6^- and $TFPB^-$ gave $K_2 \sim 10^{-4}$ M and $K_1 \sim 10^{-6}$ M, while for Cl^- an approximate value of 10^{-10} M^2 was obtained for $K = K_1 \cdot K_2$.

(82) McQuarrie, D. A. *Statistical thermodynamics*; University Science Books: New York, 1973.
(83) Seybold, P. G.; Gouterman, M. *J. Mol. Spectrosc.* **1969**, *31*, 1−13.

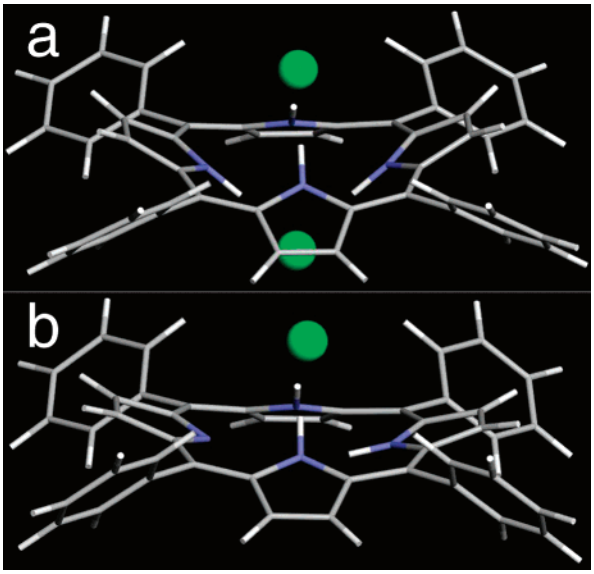

Figure 9. DFT-calculated structures of (a) $\{H_4TPP(Cl)_2\}$ and (b) $\{H_3TPP(Cl)\}$.

anions: (i) their size and the extent of charge delocalization, (ii) their hydrogen bonding ability, and (iii) their hydrophobicity. In general, we expect that poorly coordinating, large, and substantially hydrophobic species should be more effective in obtaining monoprotonated tetraaryl-porphyrins. These diacid derivatives have substantial ion-pair character, in which covalent interactions represent a significant component for the hydrogen bonding of the anions with the protonated nitrogen core.[8] For these reasons the nature of the solvent should also play a very important role. Lowering the dielectric constant of the solvent is expected to strengthen the ion-pairing process and to decrease the stability range for the *MA* species. Indeed, a recent paper has demonstrated that diprotonated tetra-*p*-tolylporphyrin species, having large and very weakly nucleophilic carborane counteranions, is the only detectable species in solutions of low-polarity solvents, such as chloroform or benzene, even if a concentration dependence study has not been reported and the higher concentration required by NMR should favor the *DA* species.[12]

It is worthwhile to briefly comment on the molecular structure of the $\{H_3TPP(Cl)\}$ *MA* species. At variance with $\{H_3TPP(PF_6)\}$, only a stable structure of C_s symmetry is theoretically predicted for $\{H_3TPP(Cl)\}$. The DFT-optimized structure of $\{H_3TPP(Cl)\}$ is displayed in Figure 9 together with that of the parent diacid (D_{2d} symmetry) previously reported.[8]

It is apparent that the $\{H_3TPP(Cl)\}$ structure closely resembles that of the **a** isomer of $\{H_3TPP(PF_6)\}$, and, similarly, it can be considered as derived from the parent diacid by removing one anion and one of the bonded NH protons. The degree of saddling and the magnitude of the tilting angle of the *meso*-phenyl rings are very similar in the two *MA* species, the replacement of PF_6 by Cl only inducing a modest but not negligible (ca. 0.02 Å) contraction of the porphyrin cavity. It is worthwhile to mention that optimization of a structure similar to that of the **b** isomer of $\{H_3TPP(PF_6)\}$ afforded a structure showing *well separated* H_2TPP and HCl subunits.

Due to the complexity of the involved effects, a deeper understanding of the electronic factors at the origin of the relative stability of the *MA*, *DA*, and *FB* species as a function of the counteranion is still an open question which deserves more investigations.

Concluding Remarks

The electronic absorption and emission studies reported in this paper suggest that normally unstable species, such as the elusive H_2TPP porphyrin monoacids, can be stabilized in low polarity solvents through the interaction with bulky and weakly coordinating anions, that are not capable of strong interactions with the protonated porphyrin macrocycle.

DFT calculations have provided structural models both for the diacid and the monoacid species, whereas TDDFT calculations with different functionals have given insight into the excited states of these species. We achieved a remarkably good description of their optical spectra, which strongly supports the assignment of the spectral features of the intermediate species to a monoacid porphyrin. We expect that the possibility to isolate monoprotonated species of the simple tetraphenylporphyrin may open the way to the identification of similar species with a large variety of porphyrins and may shed some light in fundamental understanding of the role of monoprotonated species in the coordination of metal ions into the porphyrin core.

Acknowledgment. We thank MIUR (COFIN 2004-06) for financial support and Dr. Norberto Micali (IPCF-CNR, Messina, Italy) for fluorescence lifetimes measurements.

Supporting Information Available: Deconvolution of the UV/vis spectrum of $\{H_3TPP(TFPB)\}$ (Figure SI1); 3D fluorescence data (Figures SI2 and SI3); UV/vis spectral change upon dilution of a $\{H_4TPP(PF_6)_2\}$ solution in CH_2Cl_2 (Figure SI4); UV/vis spectral change on water addition to the *MA* solution (Figure SI5); and Cartesian coordinates for optimized structures of $\{H_4TPP(PF_6)_2\}$, $\{H_3TPP(PF_6)\}$ (**a** and **b** isomers), $\{H_4TPP(Cl)_2\}$, and $\{H_3TPP(Cl)\}$. This material is available free of charge via the Internet at http://pubs.acs.org.

IC0703373